Inorg. Chem. **2008**, *47*, 12024−12031

Analysis of the Critical Step in Catalytic Carbodiimide Transformation: Proton Transfer from Amines, Phosphines, and Alkynes to Guanidinates, Phosphaguanidinates, and Propiolamidinates with Li and Al Catalysts

Christopher N. Rowley, Tiow-Gan Ong, Jessica Priem, Darrin S. Richeson,* and Tom K. Woo*

Centre for Catalysis Research and Innovation, Department of Chemistry, University of Ottawa, Ontario, Canada, K1N 6N5

Received September 9, 2008

While lithium amides supported by tetramethylethylenediamine (TMEDA) are efficient catalysts in the synthesis of substituted guanidines via the guanylation of an amine with carbodiimide, as well as the guanylation of phosphines and conversion of alkynes into propiolamidines, aluminum amides are only efficient catalysts for the guanylation of amides. Density functional theory (DFT) calculations were used to explain this difference in activity. The origin of this behavior is apparent in the critical step where a proton is transferred from the substrate to a metal guanidinate. The activation energies of these steps are modest for amines, phosphines, and alkynes when a lithium catalyst was used, but are prohibitively high for the analogous reactions with phosphines and alkynes for aluminum amide catalysts. Energy decomposition analysis (EDA) indicates that these high activations energies are due to the high energetic cost of the detachment of a chelating guanidinate nitrogen from the aluminum in the proton transfer transition state. Amines are able to adopt an ideal geometry for facile proton transfer to the aluminum guanidinate and concomitant Al−N bond formation, while phosphines and alkynes are not.

Introduction

Guanidines have a broad and growing presence in organic and inorganic chemistry.[1] The guanidine moiety is present in a variety of important natural products, which has spurred the development of a range of techniques to synthesize substituted guanidines.[2] Further, guanidines can serve as parent ligands in the synthesis of metal guanidinates,[3] which have been investigated, along with amidinates, as potential olefin polymerization catalysts[4,5] and thin film precursors.[6] One straightforward and atom economical approach to the synthesis of substituted guanidines is the addition of an amine

* To whom correspondence should be addressed. E-mail: darrin@uottawa.ca (D.S.R.), twoo@uottawa.ca (T.K.W.).

(1) (a) Mori, A.; Cohen, B. D.; Lowenthal, A. *Guanidines: Historical, Biological, Biochemical and Clinical Aspects of the Naturally Occurring Guanidino Compounds*; Plenum Press: New York, 1985; p 479. (b) Edelmann, F. T.; Anthony, F. H.; Mark, J. F. Advances in the Coordination Chemistry of Amidinate and Guanidinate Ligands. In *Advances in Organometallic Chemistry*; Academic Press: New York, 2008; Vol. *57*, pp 183−352.

(2) (a) Kent, D. R.; Cody, W. L.; Doherty, A. M. *Tetrahedron Lett.* **1996**, *37* (48), 8711–8714. (b) Yong, Y. F.; Kowalski, J. A.; Lipton, M. A. *J. Org. Chem.* **1997**, *62* (5), 1540–1542. (c) Wu, Y.-Q.; Hamilton, S. K.; Wilkinson, D. E.; Hamilton, G. S. *J. Org. Chem.* **2002**, *67* (21), 7553–7556. (d) Katritzky, A. R.; Rogovoy, B. V. *ARKIVOC* **2005**, (4), 49–87.

(3) (a) Tin, M. K. T.; Thirupathi, N.; Yap, G. P. A.; Richeson, D. S. *J. Chem. Soc., Dalton Trans.* **1999**, (17), 2947–2951. (b) Coles, M. P. *Dalton Trans.* **2006**, (8), 985–1001. (c) Findlater, M.; Hill, N. J.; Cowley, A. H. *Dalton Trans.* **2008**, (33), 4419–4423.

(4) (a) Coles, M. P.; Jordan, R. F. *J. Am. Chem. Soc.* **1997**, *119* (34), 8125–8126. (b) Coles, M. P.; Swenson, D. C.; Jordan, R. F.; Young, V. G., Jr *Organometallics* **1997**, *16* (24), 5183–5194. (c) Duncan, A. P.; Mullins, S. M.; Arnold, J.; Bergman, R. G. *Organometallics* **2001**, *20* (9), 1808–1819. (d) van Meerendonk, W. J.; Schroder, K.; Brussee, E. A. C.; Meetsma, A.; Hessen, B.; Teuben, J. H. *Eur. J. Inorg. Chem.* **2003**, (3), 427–432. (e) Bambirra, S.; Bouwkamp, M. W.; Meetsma, A.; Hessen, B. *J. Am. Chem. Soc.* **2004**, *126* (30), 9182–9183. (f) Zhang, Y.; Reeder, E. K.; Keaton, R. J.; Sita, L. R. *Organometallics* **2004**, *23* (14), 3512–3520.

(5) Aeilts, S. L.; Coles, M. P.; Swenson, D. C.; Jordan, R. F.; Young, V. G., Jr *Organometallics* **1998**, *17* (15), 3265–3270.

(6) (a) Hubert-Pfalzgraf, L. G.; Decams, J.-M.; Daniele, S. *J. Phys. IV France* **1999**, 09. (b) Carmalt, C. J.; Newport, A. C.; O'Neill, S. A.; Parkin, I. P.; White, A. J. P.; Williams, D. J. *Inorg. Chem.* **2005**, *44* (3), 615–619. (c) Milanov, A.; Bhakta, R.; Baunemann, A.; Becker, H. W.; Thomas, R.; Ehrhart, P.; Winter, M.; Devi, A. *Inorg. Chem.* **2006**, *45* (26), 11008–11018. (d) Baunemann, A.; Winter, M.; Csapek, K.; Gemel, C.; Fischer, R. A. *Eur. J. Inorg. Chem.* **2006**, (22), 4665–4672. (e) Brazeau, A. L.; Wang, Z.; Rowley, C. N.; Barry, S. T. *Inorg. Chem.* **2006**, *45* (6), 2276–2281. (f) Baunemann, A.; Bekermann, D.; Thiede, T. B.; Parala, H.; Winter, M.; Gemel, C.; Fischer, R. A. *Dalton Trans.* **2008**, (28), 3715–3722.

10.1021/ic801739a CCC: $40.75
Published on Web 11/12/2008

Scheme 1. General Catalytic Cycle for the Guanylation of Amines through the Carbodiimide Insertion - Proton Transfer Mechanism

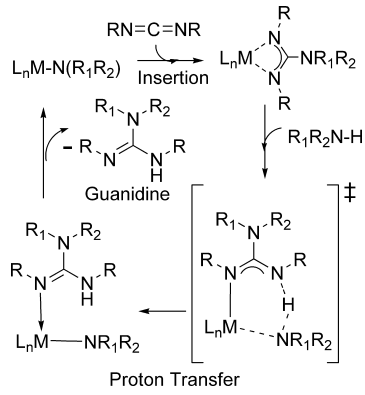

to a carbodiimide. Although some amines can undergo direct addition to carbodiimide, many synthetically important electron-deficient amines require a catalyst to facilitate the guanylation.

The first generation of guanylation catalysts featured a metal−imido bond which can undergo a [2 + 2] addition with a carbodiimide.[7,8] These catalysts are limited to primary amines and require elevated temperatures to achieve good activity. More recent examples of guanylation catalysts have featured a metal−amido bond,[9] and include amide containing alkali,[10,11] main group,[12] transition metal,[13] and lanthanide[14] guanylation catalysts. The proposed catalytic cycle for these transformations, shown in Scheme 1, begins with a carbodiimide insertion into the metal−amido bond to form a metal-guanidinate followed by a proton transfer reaction between the substrate amine and the guanidinate ligand with concomitant regeneration of a metal−amido species and release of the product guanidine. The report that TMEDA-supported lithium amides are efficient amine guanylation catalysts is particularly significant, as it demonstrates that simple and readily accessible alkali metals can function in guanylation catalysts.[10]

Recently, our group used a combination of experiment and density functional theory (DFT) calculations to investigate the catalytic cycle of the guanylation of amines with a tetramethylethylenediamine (TMEDA) supported lithium amide, identifying a mechanism consistent with the carbodiimide insertion − proton transfer mechanism discussed above. Our analysis of this mechanism led us to consider aluminum amides as potential catalysts, which have had remarkable success as transamidination catalysts[15] and for the cyclotrimerization of cyanamides.[16] We first explored the viability of aluminum amide catalysts using DFT calculations, which predicted that aluminum amides should be efficient guanylation catalysts for electron-deficient amines. We then confirmed these predictions experimentally for a range of amines.[12]

The first step of the catalytic cycle is straightforward, as carbodiimide insertions into metal−amide bonds are well-known and have been extensively studied.[8,17] The subsequent proton transfer step in the guanylation is somewhat more novel. Our earlier DFT study found that the transition state structure for this reaction step involves the detachment of one of the chelating guanidinate nitrogens from the metal, which then abstracts a proton from the amine substrate and results in simultaneous formation of a bond between the metal and the amine nitrogen.[12] This yields a Lewis acid−base complex between the metal and a neutral guanidine, which can dissociate to produce free guanidine and a metal−amido complex available for further turnovers.[18]

In addition to their activity as amine guanylation catalysts, lithium amide catalysts have also been demonstrated to be active catalysts in the guanylation of phosphines,[11] as well as reaction of alkynes with carbodiimide to yield propiolamidines,[10] demonstrating a broad scope for the proton transfer step. Similar phosphaguanylation activity was recently observed in the amides of group 2 elements Ca, Sr, and Ba.[19] Phosphaguanidines[9,11,20] and propiolamidines[21] are

(7) Ong, T.-G.; Yap, G. P. A.; Richeson, D. S. *J. Am. Chem. Soc.* **2003**, *125* (27), 8100–8101.
(8) Montilla, F.; del Rio, D.; Pastor, A.; Galindo, A. *Organometallics* **2006**, *25* (21), 4996–5002.
(9) Zhang, W.-X.; Hou, Z. *Org. Biomol. Chem.* **2008**, *6*, 10.
(10) Ong, T.-G.; O'Brien, J. S.; Korobkov, I.; Richeson, D. S. *Organometallics* **2006**, *25* (20), 4728–4730.
(11) Zhang, W.-X.; Nishiura, M.; Hou, Z. *Chem. Commun.* **2006**, (36), 3812–3814.
(12) Rowley, C. N.; Ong, T.-G.; Priem, J.; Woo, T. K.; Richeson, D. S. *Inorg. Chem.* **2008**, *47*, 9660–9668.
(13) Shen, H.; Chan, H.-S.; Xie, Z. *Organometallics* **2006**, *25* (23), 5515–5517.
(14) Zhou, S.; Wang, S.; Yang, G.; Li, Q.; Zhang, L.; Yao, Z.; Zhou, Z.; Song, H.-b. *Organometallics* **2007**, *26* (15), 3755–3761.
(15) (a) Hoerter, J. M.; Otte, K. M.; Gellman, S. H.; Stahl, S. S. *J. Am. Chem. Soc.* **2006**, *128* (15), 5177–5183. (b) Hoerter, J. M.; Otte, K. M.; Gellman, S. H.; Cui, Q.; Stahl, S. S. *J. Am. Chem. Soc.* **2008**, *128* (15), 647–654.
(16) Dornan, P.; Rowley, C. N.; Priem, J.; Barry, S. T.; Burchell, T. J.; Woo, T. K.; Richeson, D. S. *Chem. Commun.* **2008**, 3545–3647.
(17) (a) Hey-Hawkins, E.; Lindenberg, F. *Z. Naturforsch. B.* **1993**, *48* (7), 951–957. (b) Li, M.-D.; Chang, C.-C.; Wang, Y.; Lee, G.-H. *Organometallics* **1996**, *15* (10), 2571–2574. (c) Srinivas, B.; Chang, C.-C.; Chen, C.-H.; Chiang, M. Y.; Chen, I. T.; Wang, Y.; Lee, G.-H. *J. Chem. Soc., Dalton Trans.* **1997**, (6), 957–963. (d) Chang, C.-C.; Hsiung, C.-S.; Su, H.-L.; Srinivas, B.; Chiang, M. Y.; Lee, G.-H.; Wang, Y. *Organometallics* **1998**, *17* (8), 1595–1601. (e) Tunge, J. A.; Czerwinski, C. J.; Gately, D. A.; Norton, J. R. *Organometallics* **2001**, *20* (2), 254–260. (f) Zhang, J.; Cai, R.; Weng, L.; Zhou, X. *J. Organomet. Chem.* **2003**, *672* (1−2), 94–99. (g) Zhang, J.; Cai, R.; Weng, L.; Zhou, X. *J. Organomet. Chem.* **2003**, *672* (1−2), 94–99. (h) Hill, N. J.; Moore, J. A.; Findlater, M.; Cowley, A. H. *Chem. Commun.* **2005**, (43), 5462–5464. (i) Rowley, C. N.; DiLabio, G. A.; Barry, S. T. *Inorg. Chem.* **2005**, *44* (6), 1983–1991. (j) Findlater, M.; Hill, N. J.; Cowley, A. H. *Polyhedron* **2006**, *25* (4), 983–988. (k) Pierce, G. A.; Coombs, N. D.; Willock, D. J.; Day, J. K.; Stasch, A.; Aldridge, S. *Dalton Trans.* **2007**, (39), 4405–4412.
(18) The crystallographic structure of a similar complex has been reported. Coles, M. P.; Hitchcock, P. B. *Chem. Commun.* **2005**, (25), 3165–3167.
(19) Crimmin, M. R.; Barrett, A. G. M.; Hill, M. S.; Hitchcock, P. B.; Procopiou, P. A. *Organometallics* **2008**, *27* (4), 497–499.
(20) (a) Issleib, K.; Schmidt, H.; Meyer, H. *J. Organomet. Chem.* **1980**, *192* (1), 33–39. (b) Grundy, J.; Coles, M. P.; Hitchcock, P. B. *Dalton Trans.* **2003**, (12), 2573–2577. (c) Grundy, J.; Coles, M. P.; Avent, A. G.; Hitchcock, P. B. *Chem. Commun.* **2004**, (21), 2410–2411. (d) Mansfield, N. E.; Coles, M. P.; Hitchcock, P. B. *Dalton Trans.* **2005**, (17), 2833–2841. (e) Mansfield, N. E.; Coles, M. P.; Avent, A. G.; Hitchcock, P. B. *Organometallics* **2006**, *25* (10), 2470–2474. (f) Mansfield, N. E.; Coles, M. P.; Hitchcock, P. B. *Dalton Trans.* **2006**, (17), 2052–2054. (g) Grundy, J.; Mansfield, N. E.; Coles, M. P.; Hitchcock, P. B. *Inorg. Chem.* **2008**, *47* (7), 2258–2260.
(21) (a) Himbert, G.; Schwickerath, W. *Liebigs Ann. Chem.* **1984**, (1), 85–97. (b) Xu, X.; Gao, J.; Cheng, D.; Li, J.; Qiang, G.; Guo, H. *Adv. Synth. Catal.* **2008**, *350* (1), 61–64.

valuable synthetic targets in their own right and their catalytic synthesis will facilitate further exploration of their structures and activities. Based on our success using aluminum amides as amine guanylations catalysts, we attempted to use the aluminum amides to catalyze the guanylation of phosphines and the propiolamination of alkynes. In contrast to the success seen with lithium amide catalysts in these reactions, all our experimental attempts to catalyze the propiolamination of alkynes and the guanylation of phosphines with aluminum amides resulted in very poor or no activity.[22]

In this report, we have used DFT calculations to explore the origin of the difference in catalytic activity observed with the Li- and Al-amide catalysts. More specifically, we have examined the transition state structures and activation energies for the guanylation (or propioamidination) of three representative substrates (aniline, phenylphosphine, and ethyne) with TMEDA-Li and dichloro aluminum catalysts. The data from these calculations lead us to consider differences in the nature of the metal-bonding in the two systems. As a result, we have used energy decomposition analysis (EDA)[23] to further identify why lithium amides are able to catalyze the guanylation of amines and phosphines as well as the propiolamidination of alkynes, while aluminum amide is only an active catalyst for the guanylation of amines and not the other two substrates.

Results and Discussion

Literature precedence[10,24] and our own calculations[12,25] have established that carbodiimide can insert readily into lithium and aluminum amido, phosphido, and acetylide bonds. The critical reaction step occurs in the second leg of the catalytic cycle (Scheme 1), where the metal-guanidinate, phosphaguanidinate, or propiolamidinate accepts a proton from the substrate. The transfer of the proton occurs through a transition state where the substrate coordinates to the metal center and one of the coordinating nitrogens of the chelating ligand detaches from the metal and accepts a proton from the substrate. Here, sharp distinctions can be drawn between the lithium and aluminum systems as well as the amine, phosphine, and alkyne substrates. In the next section we examine the reaction profile for the proton transfer reactions with the TMEDA-Li catalyst. Following that section, the same is done for the dichloro aluminum catalyst and a comparison is made. These sections are then followed by a detailed EDA analysis of specific transition states and intermediates of the proton transfer in order to obtain a deeper understanding of the reactivity differences of the catalysts.

Lithium Complexes. Our examination into the origin of the differences in the substrate dependent catalytic abilities of lithium and aluminum species began with optimized

Scheme 2. Proton Transfer Reactions Modeled for Lithium Complexes

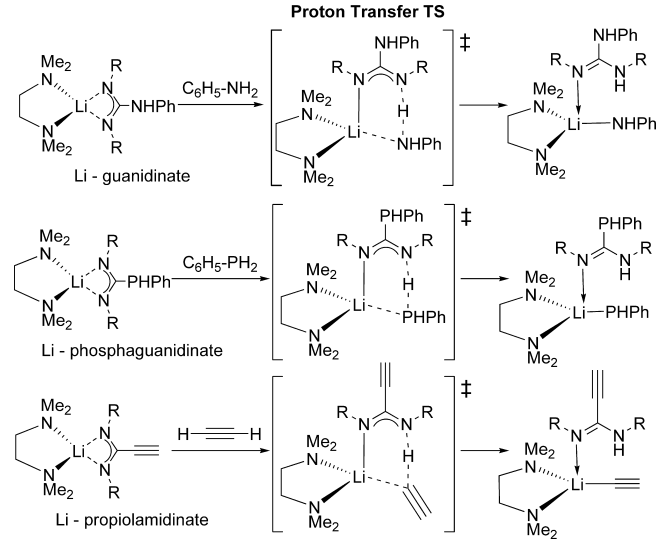

transition state structures of the critical proton transfer step between different three representative substrates, aniline, phenylphosphine, and ethyne with the corresponding lithium guanidinate, phosphaguanidinate, or propiolamidinate (Scheme 2, Figure 1, Table 1). The transition state geometries with the aniline, phenylphosphine, and ethyne substrates are similar, although the transition state for aniline proton transfer occurs late on the reaction coordinate, when the N(guanidinate)−H distance is 1.30 Å. The corresponding distance for phenylphosphine is 1.54 Å and it is 1.40 Å for ethyne.

The proton transfer with aniline ($C_6H_5-NH_2$) has a considerably lower barrier than for phenylphosphine, despite the greater N−H bond strength of aniline. In the case of aniline, the activation energy of the proton transfer reaction is only 11.0 kcal mol^{-1}, while the activation energy is higher for proton transfer from phenylphosphine (18.5 kcal mol^{-1}) or ethyne (15.8 kcal mol^{-1}). This difference stems from the strength of the developing metal-substrate bond. In the case of aniline, the nitrogen center is 2.07 Å from the lithium at the transition state, allowing it to have a significant bonding interaction at the transition state. In contrast, for the proton transfer from phenylphosphine, the Li−P bond distance is 2.86 Å, with a much weaker bonding interaction. The proton transfer reaction with ethyne has a barrier similar to that of phenylphosphine. The bond that forms between the ethyne substrate and the lithium center is also weaker and originates from the sp hybridized orbital of the C−H bond involved in proton transfer rather than the ethyne π-orbitals. As a result, the Li−C bond is only formed to a limited degree at the transition state, again reflecting the fact that the proton transfer is the energetically dominant process.

The proton transfer step leads to a complex where the newly formed neutral guanidine, phosphaguanidine, or propiolamidine is coordinated to lithium via the lone pair of the sp^2 hybridized nitrogen. All three reactions are approximately thermoneutral, with reaction energies near 0 kcal mol^{-1} (defined as the difference of the absolute Gibbs free energy of the product complex and the reactants). This

(22) Ong, T.-G., Priem, J., Richeson, D. S. unpublished results.
(23) Bickelhaupt, F. M.; Baerends, E. J. Kohn-Sham Density Functional Theory: Predicting and Understanding Chemistry. In *Rev. Comput. Chem*; Wiley-VCH: New York, 2000; Vol. *15*, pp 1−86.
(24) (a) Richter, J.; Feiling, J.; Schmidt, H.-G.; Noltemeyer, M.; Brueser, W.; Edelmann, F. T. *Z. Anorg. Allg. Chem.* **2004**, *630* (8−9), 1269–1275. (b) Hill, N. J.; Findlater, M.; Cowley, A. H. *Dalton Trans.* **2005**, (19), 3229–3234. (c) Otero, A.; Fernandez-Baeza, J.; Antinolo, A.; Tejeda, J.; Lara-Sanchez, A.; Sanchez-Barba, L. F.; Lopez-Solera, I.; Rodriguez, A. M. *Inorg. Chem.* **2007**, *46* (5), 1760–1770.

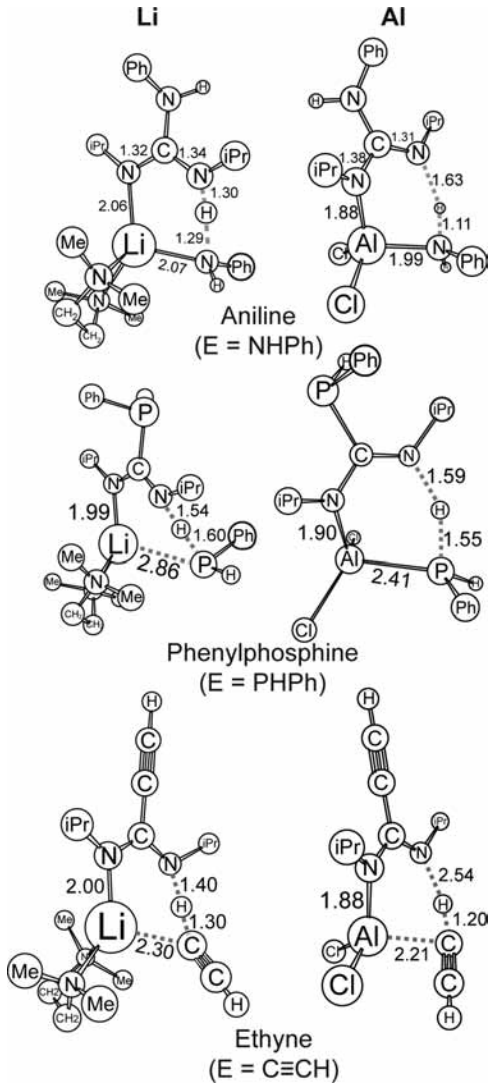

Figure 1. Schematic structures of proton transfer transition states for the reaction of TMEDA-lithium (left) and Cl_2Al- (right) guanidinate, phosphaguanidinate, and propiolamidinate with substrates aniline, phenylphosphine, and ethyne, respectively.

Table 1. Calculated Gibbs Free Energies of Activation for the Proton Transfer Step of the Guanylation of Aniline, Phenylphosphine, and Ethyne for TMEDA-Li- and Cl_2Al-Catalysts

	activation energy (kcal mol^{-1})		reaction energy (kcal mol^{-1})	
substrate	Li	Al	Li	Al
aniline	11.0	16.5	0.1	0.2
phenylphosphine	18.5	26.6	0.2	1.1
ethyne	15.8	30.7	−0.1	0.1

complex can readily undergo dissociation, releasing the product and regenerating the active catalyst.

Aluminum Complexes. We next calculated transition state structures for the analogous proton transfer reaction between a dichloroaluminum guanidinate, phosphaguanidinate, and propiolamidinate with the substrates aniline, phenylphosphine, and ethyne, respectively (Scheme 3, Figure 1, Table 1). At the transition state, the aluminum center is in a tetrahedral coordination mode with asymmetric Al−N bonds (1.88 Å for the Al−N(guanidinate) bond vs 1.99 Å for the Al−N(amide) bond). The barrier of the proton transfer with

Scheme 3. Proton Transfer Reactions Modeled for Aluminum Complexes

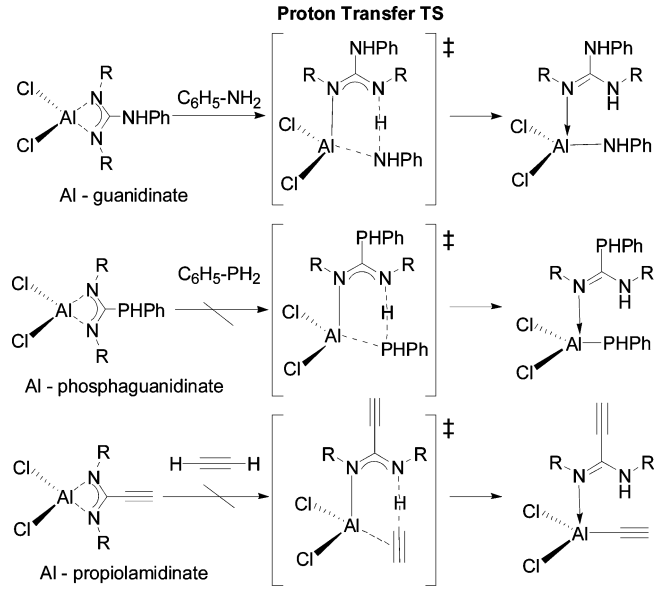

this transition state is larger than the analogous transfer with the lithium catalyst but remains modest (16.5 kcal mol^{-1}).

As we observed with the lithium reactions, the activation energies of the proton transfer reactions with phenylphosphine and ethyne are much larger than for aniline, with barriers of 26.6 and 30.7 kcal mol^{-1}, respectively (Table 1). The transition state geometry in the case of phenylphosphine is similar to that of aniline (Figure 1), with a proton being transferred from the coordinated phosphine to the nitrogen center. The aluminum phosphorus bond is almost fully formed at the transition state (2.41 Å in the TS vs 2.39 Å in the product complex), in contrast to the analogous lithium reaction, where the Li−P bond is only partially formed at the TS (Li−P = 2.86 Å). The proton transfer reaction with ethyne is consistent with abstraction of a proton from the ethyne by the propiolamidinate ligand and concomitant formation of an Al−C bond. At the transition state, the incoming ethyne interacts with the aluminum through its π orbitals, as indicated by the Al−C≡C angle of 88°, instead of through the C−H sp orbital as in the analogous lithium reaction.

As observed with the lithium reactions, the three reactions with aluminum lead to complexes where the newly formed neutral guanidine, phosphaguanidine or propiolamidine is coordinated to the aluminum center via the lone pair of the sp^2 hybridized nitrogen and the guanidine N−H bond forms a hydrogen bond with the anionic ligand. Likewise, the reaction energies indicate that this reaction is approximately thermoneutral, as for the lithium catalysts. This hydrogen bonding interaction is weaker than in the lithium complexes because the aluminum phosphido and aluminum alkynyl bonds are less polarized.

Transition State Bond Energy Analysis. With the aim of obtaining a more intimate understanding of the trends in the proton transfer activity, we applied EDA, a technique used to calculate the magnitude and nature of bonding between two constituent fragments of a complex.[23] In this

Table 2. EDA of the Proton Transfer Transition State with Aniline, Phenylphosphine, Ethyne and the Corresponding (Phospha)guanidinate or Propiolamidinate for Lithium and Aluminum (kcal mol^{-1})

bond energy component (kcal mol^{-1})		(L)M = $NMe_2-CH2-CH_2NMe_2$)Li(^{i}PrNC(E)N^{i}Pr)			(L)M = Cl_2Al (^{i}PrNC(E)N^{i}Pr)		
		E = NHPh	E = PHPh	E = C′CH	E = NHPh	E = PHPh	E = C′CH
preparation energy	metal	15.0	10.6	11.5	43.6	42.5	38.0
	substrate	23.8	7.1	23.0	4.2	14.4	6.9
electrostatic		−80.3	−42.9	−50.3	−104.2	−93.7	−69.3
Pauli		122.7	81.3	90.4	132.9	141.2	120.6
net steric		42.4	38.4	40.1	28.7	47.5	51.3
orbital interactions		−85.0	−47.9	−65.1	−74.3	−85.8	−77.7
total bond energy		−42.6	−9.5	−25.0	−45.6	−38.3	−26.4
total interaction energy		−3.8	8.2	9.5	2.2	18.6	18.5

technique, the net interaction energy between two fragments is calculated. This interaction energy is divided into components of steric interaction and orbital interactions. The steric interaction is the sum of the electrostatic interactions and Pauli repulsion of the two fragments. The orbital interaction component reflects the degree of overlap between the orbitals of the two fragments. Additionally, each fragment must distort from the minimum energy geometry of its free species to its geometry in the complex. The last contribution to the interaction energy is the preparation energy, which is the difference in electronic energy of the fragment in its minimum energy configuration and the configuration it holds in the complex, which counters part of the favorable bonding interactions experienced in the complex. The data for this analysis are presented in Table 2.

We assigned the atoms of the proton transfer transition state structures into two neutral fragments: the metal fragment, containing the atoms from the metal, auxiliary ligands, (phospha)guanidinate or propiolamidinate, and a substrate fragment, containing the amine, phosphine, or alkyne substrate (Figure 2). We use the abbreviation E to refer to the fragment of the substrate transferring the proton to the metal (phospha)guanidinate or propiolamidinate.

Table 2 reveals that the preparation energies for the lithium metal fragments are significantly lower than for the analogous aluminum metal fragments. This suggests that the lithium (phospha)guanidinates and propiolamidinates are able to distort to the transition state geometry without incurring a large energetic penalty (vide infra). The substrate preparation energies vary widely for both substrates and metals. It is more difficult to extract chemically significant data from these energies because the preparation energies of these fragments is largely dependent on the degree of bond breaking for the substrate E−H bond that is involved in the proton transfer step. In the case of lithium, the proton transfer reaction with aniline and ethyne have late transition states. This means that the N−H and C−H bonds that are broken in the abstraction are stretched dramatically from their equilibrium geometries (Figure 1).

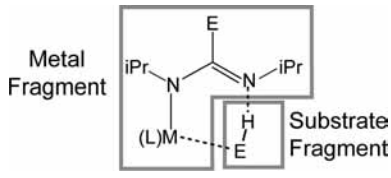

Figure 2. Fragments used in the EDA analysis of the proton transfer transition state.

The steric and orbital interactions contributions are markedly different for the aluminum complexes compared to the analogous lithium compounds. For example, the proton transfer transition state between the lithium complex and aniline has higher steric interactions but lower orbital interactions than that of the corresponding aluminum species. The opposite trend is observed for the proton transfers with phenylphosphine and ethyne. The net interaction results in modest barriers for the proton transfer reactions between the lithium compounds and phenylphosphine or ethyne, but prohibitively high barriers for the related reactions with the aluminum species.

In contrast to the high activation energies seen in the proton transfer step for phenylphosphine and ethyne, the activation energy for the proton transfer from aniline to the aluminum guanidinate is modest (16.5 kcal mol^{-1}). Examination of the transition state geometry for the proton transfer reaction with aniline compared to phenylphosphine indicates that in both cases, the preferred geometry orients the E−H bond at an approximately 90° angle with respect to the metal (Figure 3). This results in the nitrogen atom of the amine substrate having a coordination mode between trigonal pyramidal and planar. In the case of free aniline, the conjugation between the π system of the phenyl group and the nitrogen center results in a nearly planar amine, with a degree of pyramidalization (DP)[26,27] of only 20%. The amine is moderately more planar at the transition state, with a DP of 7%, although the small preparation energy (4.2 kcal mol^{-1}) of the aniline fragment indicates that this distortion has a minor energetic cost. Due a greater degree of repulsion between the phosphorus lone pair and the substituents, the

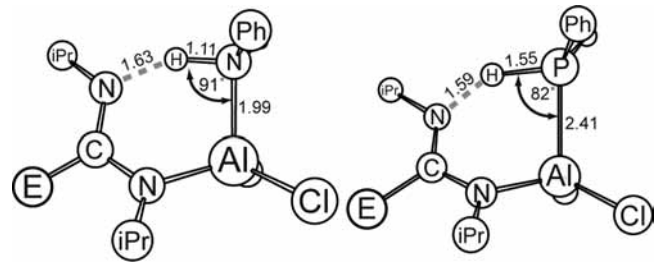

Figure 3. A comparison of the transition state geometries for the proton transfer from aniline (left) and phenylphosphine (right) with Al catalysts.

P-center of free phenylphosphine is in a trigonal pyramidal geometry, with a DP of 82%. At the transition state, the phosphorus adopts a much more planar arrangement in order to have an appropriate geometry to undergo proton transfer, with a degree of pyramidalization of 28%. The energetic cost of this deformation is apparent in the preparation energy of the phenylphosphine at the proton transfer transition state (Table 2), which is 10.2 kcal mol^{-1} higher than the preparation energy of aniline. This can be directly correlated to the electronic structure of the phenylphosphine ligand, as the HOMO of the phenylphosphine, corresponding to the phosphine lone pair, is raised in energy by 19 kcal mol^{-1} in the transition state fragment. This is in stark contrast to the molecular orbital energies of aniline, which are not dramatically changed in the aniline transition state fragment.

The proton transfer step with ethyne as the substrate is notably different than that observed for either aniline or phenylphosphine, as the aluminum center is interacting with the π orbitals of ethyne at the transition state rather than the lone pair of aniline or phenylphosphine. The preparation energies of the fragments are actually the lowest of the three substrates, as the ethyne is small enough to adopt the transition state geometry without a large distortion. Although the orbital interactions for the proton transfer step with ethyne are actually more favorable than for aniline, the steric interactions are poor, notably in terms of electrostatic interactions, which are a full 34.9 kcal mol^{-1} less favorable than for aniline. This reflects the ability of aniline and phenylphosphine to partially form ionic bonds at the transition state through their lone pairs, while ethyne has more limited interactions with the aluminum through its π orbitals.

Guanidinate Bond Energy Analysis. Having established that lithium phosphaguanidinates and propiolamidinates will undergo proton transfer with phosphines and alkynes, respectively, due to the ability of the lithium−ligand complex to distort to the proton transfer transition state structure with a small preparation energy, we next set out to determine the origin of this smaller preparation energy in electronic structure. The proton transfer requires an initial dissociation of one of the chelating nitrogen centers from the metal along with a significant structural distortion in order to accept a proton from the substrate. Consequentially, we anticipated that the energetic cost of this dissociation would be correlated to the strength of the bonding between the bidentate ligand and the metal. To determine the strength of this interaction, we performed EDA on the aluminum and lithium species that possessed either a (phospha)guanidinate or a propiolamidinate ligand in order to calculate the bond energy between the ligand and the metal. The two fragments for EDA were defined as an anionic fragment comprised of the bidentate ligand and a cationic fragment comprised of the metal and remaining ligands (Figure 4). As in the EDA of the proton transfer transition state, this analysis also divides the bond energy into components that indicate the nature of the bonding. The data from this analysis are presented in Table 3.

The three lithium complexes displayed very similar total bonding energies that are within a 2 kcal mol^{-1} range of each other. The bond energy components are also distributed in a similar range with respect to one another. This reflects the primarily ionic character of the Li(I)-guanidinate bonding. This ionic character is also evident in the preparation energies of the fragments, which are all in the 2−3 kcal mol^{-1} range, indicating that the metal and bidentate ligand geometries in the complex remain close to the geometries of their free, ionic forms.

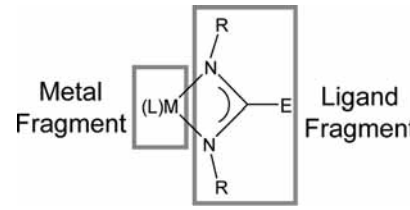

Figure 4. Fragments used in the EDA of the metal−ligand complexes.

In contrast, the aluminum complexes display a somewhat larger range of bond energies. The guanidinate with the N-phenyl exocyclic group has an interaction energy that is more than 10 kcal mol^{-1} stronger than the phosphaguanidinate or the propiolamidinate. The guanidinate has similar orbital interaction energies to the phosphaguanidinate, but more favorable steric interactions. Conversely, the propiolamidinate has similar steric interactions as the guanidinate but weaker orbital interactions.

A much larger distinction can be made between Al(III)-ligand and Li(I)-ligand bonding. The total bonding energies for the aluminum species are more than a factor of 2 higher than the corresponding lithium complexes. More specifically, the orbital interaction energies are 140 kcal mol^{-1} more favorable for the aluminum compounds reflecting the much greater degree of covalent bonding between the Al(III) metal and the bidentate ligands. Another result of the larger covalent character of this bonding in the aluminum compounds is the large preparation energies of the ligand fragments, which range from 9 to 15 kcal mol^{-1}. This is in part due to the smaller bite angle of the bidentate ligands for the Al compounds, a feature arising from the more localized, covalent bonding to the sp^3 hybridized orbitals of the aluminum center. The preparation energies of the metal fragments are consistently in the 20 kcal mol^{-1} range because the $AlCl_2^+$ fragment adopts a ~120° angle in the complexes, while the minimum energy geometry of the $AlCl_2^+$ fragment is linear. The net steric interaction also contributes more favorably to bonding in the aluminum species, due to the greater cationic character of the aluminum.

The stronger bonding between the bidentate ligands and aluminum in comparison to lithium provides a basis for explaining the differing reactivity toward proton transfer of the aluminum vs the lithium species. The weaker bonding in the case of lithium leads to complexes that are generally more reactive, while the predominately ionic character of the bonding allows for the bidentate ligand to be more easily distorted from its equilibrium geometry. In contrast, the aluminum bonds more strongly to the ligand, causing the aluminum complexes to be less reactive. Furthermore, the aluminum-ligand bonding has substantial covalent character that restricts the geometry of the complex to remain near a

Table 3. EDA of the Aluminum and Lithium Guanidinate, Phosphaguanidinate, and Propiolamidinate Complexes (kcal mol^{-1})[a]

bond energy component		(L)M = ($NMe_2CH_2CH_2NMe_2$)Li			(L)M = Cl_2Al		
		E = NHPh	E = PHPh	E = C′CH	E = NHPh	E = PHPh	E = C′CH
preparation energy	metal	3.4	3.2	3.0	24.1	22.9	24.1
	ligand	2.4	2.0	1.3	14.8	9.7	8.6
electrostatic		−126.3	−123.6	−126.5	−273.7	−256.4	−263.3
Pauli		24.6	24.7	23.8	154.4	147.2	146.7
net steric		−101.7	−98.9	−102.7	−119.3	−109.1	−116.6
orbital interactions		−32.3	−33.1	−31.2	−174.2	−172.6	−165.7
total bond energy		−134.0	−132.0	−133.9	−293.4	−281.8	−282.4
total interaction energy		−128.2	−126.8	−129.6	−254.5	−249.2	−249.7

[a] The fragments are shown in Figure 4.

tetrahedral geometry. This, in turn, leads to preparation energies for the distortion experienced at the proton transfer transition state that are much larger in the case of the aluminum-based catalysts when compared to the lithium species. These higher preparation energies result in high activation energies for the proton transfer reaction of aluminum guanidinates with phosphines and alkynes.

Guanidinate Resonance Forms. This analysis also provides insight into the magnitude of the contributions from the three dominate resonance forms present in metal-guanidinate bonding. Equal contributions of resonance forms **R1** and **R2** result in the delocalized guanidinate π system and symmetric coordination of the chelating nitrogens to the ligand. For both metals, the guanidinates, phosphaguanidinates, and propiolamidinates all coordinate in this fashion. In guanidinates, there can also be a significant contribution from **R3**, where the exocyclic nitrogen takes on a positive charge, allowing the ligand to coordinate in a dianionic fashion. This resonance form is apparent in the XRD structure of Ti{η^2-$(NPh)_2CNEt_2$}, reported by Bailey et al.,[28] where the chelating guanidinate nitrogens take on a pyramidal geometry, consistent with the sp^3 hybridization found in **R3**. This effect was also reported in the aluminum guanidinate $Cl_2Al\{^iPr_2CNMe_2\}$ by Aeilts et al.,[5] where the sum of angles of the coordinating nitrogens was 348°.

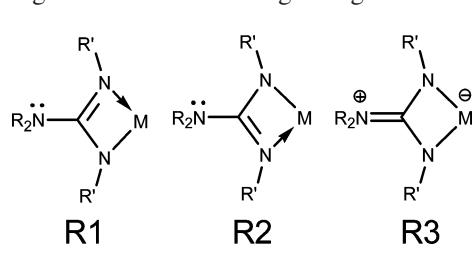

The optimized structure of the lithium guanidinate complex shows that the chelating nitrogens are nearly planar, with a sum of angles of 356°, consistent with resonance forms **R1** and **R2** dominating. The chelating nitrogens in the aluminum guanidinate show a greater degree of pyramidalization due to contributions from **R3**, with a sum of angles of 352°, consistent with the greater electron deficiency of Al(III) in comparison to Li(I). Our EDA analysis allows us to quantify the energetic benefit of this effect (Table 3). The lithium guanidinate, phosphaguanidinate, and propiolamidinate have similar total metal−ligand bond energies, restricted to a 2 kcal mol^{-1} range. In contrast, the total metal-guanidinate bond energy in the aluminum complex is 6 kcal mol^{-1} higher than the phosphaguanidinate or the propiolamidinate, indicating the **R3** resonance form contributes roughly this amount to the stabilization of this metal guanidinate.

Conclusions

DFT calculations show that the proton transfer step determines whether lithium amide or aluminum amide catalysts are efficient catalysts in the guanylation of amines. Lithium amides are effective catalysts for the guanylation of phosphines and the propiolamidination of alkynes, and the calculated activation energies of all these steps are low. In contrast, aluminum amides are poor phosphaguanylation and propiolamidination catalysts, corresponding to high activation energies for the proton transfer step with these substrates. Analysis of the proton transfer transition state structures and chemical bonding show that phosphines do not readily adopt the nearly planar geometry required for proton transfer to the phosphaguanidinate ligand and that the π system of alkynes is not able to effectively form a bond with the aluminum during proton transfer. EDA analysis indicates that lithium complexes are able to undergo proton transfer with all three substrates because the metal−ligand interaction is weak and largely ionic; the nondirectionality of the lithium-ligand binding allows these complexes to take on geometries that enable facile proton transfer. In contrast, aluminum-guanidinate bonding is much stronger, largely covalent, and directional, so these complexes are only reactive toward amines.

Detaching a chelating nitrogen from the metal incurs a large energetic cost that must be compensated for by strong metal-substrate bonding. The activation energies calculated for the reaction between aluminum guanidinates and amines are notably low, as the geometry of the proton transfer transition state is ideal and the amine is able to form a significant bonding interaction with the metal. Substrates such as phosphines and alkynes, which lack the appropriate

(25) We have modeled the carbodiimide insertion into M-NHPh, M-PHPh, and M-CCH (M = TMETA-Li, Cl2-Al) and found that the insertions are facile in each case.
(26) DP(%) = $[360 - \sum_{i=1}^{3} \alpha_i]/0.9$.
(27) Maksic, Z. B.; Kovacevic, B. *J. Chem. Soc., Perkin Trans. 2* **1999**, 6.
(28) Bailey, P. J.; Grant, K. J.; Mitchell, L. A.; Pace, S.; Parkin, A.; Parsons, S. *Dalton Trans.* **2000**, (12), 1887–1891.

geometric and electronic properties, are expected to show less reactivity toward other metal (phospha)guanidinates or amidinates with strongly covalent metal−ligand bonding.

To a limited degree, these results may speak to the broader reactivity of metal amidinates and guanidinates, which could have implications for the use of these ligands as ancillary ligands in catalysts and in thin film deposition. Complexes with predominantly ionic metal-guanidinate bonding, such the lithium guanidinate, will more readily undergo a distortion where one of the chelating guanidinate nitrogens detaches from the metal to accept a proton from a substrate, while metal-guanidinates with stronger and more covalent bonding will be less reactive.

Computional Methods

The calculations presented here were made with DFT,[29] as implemented in Turbomole 5.9[30] using the PBE functional[31] and the def2-TZVPP basis set.[32] Ziegler-Morokuma EDA analysis was performed by reoptimizing the complexes in ADF 2005.1 with the PBE functional and the TZP basis set. Solvent effects were not found to be significant when a COSMO continuum solvent model was applied, so all values reported in this paper are gas phase energies.

Acknowledgment. We thank NSERC of Canada and the Canada Research Chairs program for funding. CNR thanks NSERC for a PGS scholarship and HPCVL for research scholarships. We are also grateful to CFI, the Ontario Research Fund, IBM Canada, HPCVL and SharcNet for providing computing resources.

Supporting Information Available: Details of the computational methods, Cartesian coordinates of the optimized species, data from the calculations on the insertion stage of the catalytic cycle. This material is available free of charge via the Internet at http://pubs.acs.org.

IC801739A

(29) Ziegler, T.; Autschbach, J. *Chem. Rev.* **2005**, *105* (6), 2695–2722.
(30) Ahlrichs, R.; Baer, M.; Haeser, M.; Horn, H.; Koelmel, C. *Chem. Phys. Lett.* **1989**, *162* (3), 165–9.
(31) Perdew, J. P.; Burke, K.; Ernzerhof, M. *Phys. Rev. Lett.* **1996**, *77* (18), 3865–3868.
(32) Weigend, F.; Ahlrichs, R. *PCCP* **2005**, *7* (18), 3297–3305.